

A Large Particle Associated with the Perimeter of the Nuclear Pore Complex

P. N. T. UNWIN and R. A. MILLIGAN

Department of Structural Biology, Stanford University Medical School, Stanford, California 94305; and Medical Research Council Laboratory of Molecular Biology, Cambridge, England

ABSTRACT The three-dimensional structure of the nuclear pore complex has been determined to a resolution of ~ 90 Å by electron microscopy using nuclear envelopes from *Xenopus* oocytes. It is shown to be an assembly of several discrete constituents arranged with octagonal symmetry about a central axis. There are apparent twofold axes perpendicular to the octad axis which suggest that the framework of the pore complex is constructed from two equal but oppositely facing halves. The half facing the cytoplasm is in some instances decorated by large particles, similar in appearance and size to ribosomes.

The nuclear pore complex is an organelle, ubiquitous to eucaryotic cells, which serves as a pathway through the nuclear envelope for a variety of nuclear and cytoplasmic molecules. Microinjection experiments involving substances such as dextrans (24), colloidal gold (10), and proteins (4, 7, 16) suggest that it forms an opening for passive movement of molecules up to ~ 90 Å in diameter. Biochemical studies suggest that it may be composed of only a few major polypeptides (19) and may contain RNA (28), although no direct identification has yet been achieved of these components within the confines of the structure. Besides this knowledge, very little information is available on the chemical or physical nature of the constituents or of their mechanisms of action.

Electron microscopy shows that the pore complex is a cylindrical assembly spanning the two nuclear membranes and having components arranged with octagonal symmetry around its central axis (6, 9, 12, 14). However, the details described by different authors vary considerably, probably because of real differences associated with the cell cycle and also because of artifactual differences related to quality of preservation.

Here we have investigated the structure of pore complexes from *Xenopus* oocytes using Fourier averaging methods to reveal the details. Additional information obtained by selectively releasing some of the constituents has led to a clearer picture of their organization and of the overall three-dimensional configuration. Our results emphasize the subunit nature of the pore complex and we show that particles similar in appearance and size to ribosomes associate with its cytoplasmic perimeter.

MATERIALS AND METHODS

General

Nuclear envelopes used were from the oocytes of *Xenopus laevis*. The oocytes were kept in small ovary pieces in modified Barth's saline solution (15) at 17°C for periods up to several days. Chemicals were obtained from the following sources: triethanolamine chloride from BDH Chemicals Ltd. (Poole, England); poly-L-Lysine (40,000 mol wt) and gold thio-glucose from Sigma Chemical Co. (St. Louis, MO); glutaraldehyde (ultrapure) from Emscope Laboratories (London, England); Triton X-100 from Bio-Rad Laboratories (Richmond, CA).

Low salt medium was 0.5 mM MgCl₂ in 1 mM triethanolamine chloride adjusted to pH 8 with KOH. High salt medium was 400 mM KCl, 5 mM MgCl₂, 20 mM triethanolamine chloride, adjusted to pH 8 with KOH. All solutions were prepared with double-distilled water.

Isolation of Nuclear Envelope

Nuclei were isolated from mature oocytes directly into the Barth medium by extruding them through small holes punched in the center of the oocyte black hemispheres. Each nucleus, after isolation, was cleaned by several passes up and down a narrow capillary and immediately transferred to an electron microscope grid.

Isolation of Ribosomes

To compare particles on the nuclear envelope with particles known to be ribosomes, we used as markers ribosomes isolated from hypothermic chick embryos (which have about the same molecular weight as those from *Xenopus* [20]). The ribosomes were isolated as tetramers from a postmitochondrial supernatant following, with modifications, the procedure described in (23), and they were shown to be undegraded in terms of their two-dimensional gel electrophoresis patterns (Milligan and Unwin, manuscript in preparation).

Sample Preparation

The pore complex constituents were examined *in situ*, attached to the nuclear membranes, and also in isolation, detached from them. For the first purpose we used 600-mesh grids overlaid with a holey carbon support film, and the capillary was withdrawn to leave the nucleus behind within a small hemispherical droplet on one surface. With two fine, but blunted, glass needles, the envelope was disrupted to release the nuclear contents and spread across the surface, cytoplasmic face in contact. Once firmly adhered, the envelope was washed in low salt medium (~30 s), fixed with 2.5% glutaraldehyde in the same medium (1 min), and postfixed with 1% osmium tetroxide (1 min). These and subsequent steps were carried out with the grid completely immersed so that both sides received the same treatments. In some experiments, we carried out an additional incubation for 1 min in high salt, or in low salt with the $MgCl_2$ replaced by 1 mM ethylenediaminetetraacetic acid (EDTA), between the washing and fixation steps.

For the second purpose we used normal carbon-coated grids which had been rendered hydrophilic on one surface by bathing in 0.1% polylysine (34). Each grid was placed on parafilm, hydrophilic side uppermost, and immersed in a droplet of low salt medium (sometimes containing 0.1% Triton X-100) before the nucleus was delivered onto it. After its attachment to the grid, the envelope was disrupted, partially spread as described above, and centrifuged at 500 g for 1 min. The envelope was then partially detached from the grid by vigorous swirling in high salt medium (or low salt medium when Triton X-100 was used), leaving behind various constituents. A small proportion of pore complexes were released intact when Triton X-100 was used.

Staining was done in the usual way (8) using 2% gold thio-glucose or 1% uranyl acetate. The former stain gave noticeably better preservation of the nuclear envelope; otherwise, at the resolution of this study, both stains gave equivalent results. Fixation with glutaraldehyde was avoided when uranyl acetate was used.

Electron Microscopy and Image Processing

Micrographs were recorded at $\times 12,000$ – $20,000$ using a Philips EM301 or EM400 electron microscope operating at 80 kv. A goniometer stage was used for the tilting experiments. Nuclear envelopes were viewed with their cytoplasmic side nearest to the electron source.

Images of the pore complex were analyzed by numerical Fourier methods. Those images displaying the most perfect eightfold rotational symmetry were assumed to best represent the true structure. By this criterion, and for pore complexes attached to the nuclear membranes, good preservation was achieved only in regions overlying holes in the carbon support film, and in parts where the stain was sufficiently deep that the space between the pores was of uniform density.

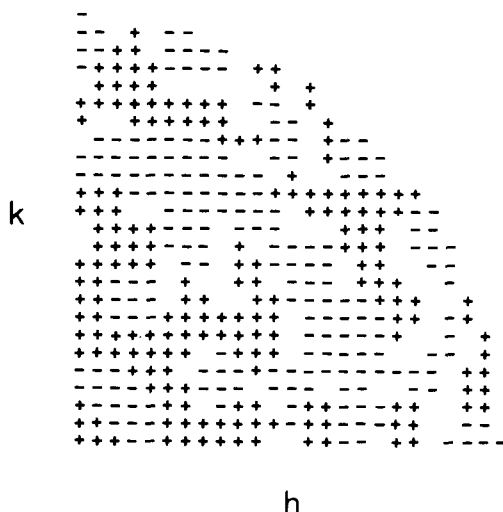


FIGURE 1 Plot of centrosymmetric phases (plus and minus are 0° and 180°) in the Fourier transform calculated from an image of a pore complex attached to the nuclear membranes. The plot was obtained by sampling the continuous transform on a square lattice at intervals of $4.34 \times 10^{-4} \text{ \AA}^{-1}$ and averaging the complex values at these points, (h, k) , with additional values collected at the eightfold related positions. The projection computed using these phases and averaged amplitudes is identical to the one in Fig. 9 a, derived by harmonic analysis of the same data.

TABLE I
Details of Three-dimensional Data Refinement

| | |
|-----------------------------------------------------------------------------------|-------------------|
| Number of images | 10 |
| Range in angle of tilt | 0 – 52° |
| Resolution cut-off | 130 \AA |
| Average phase error, based on comparison of individual values along lattice lines | 29° |

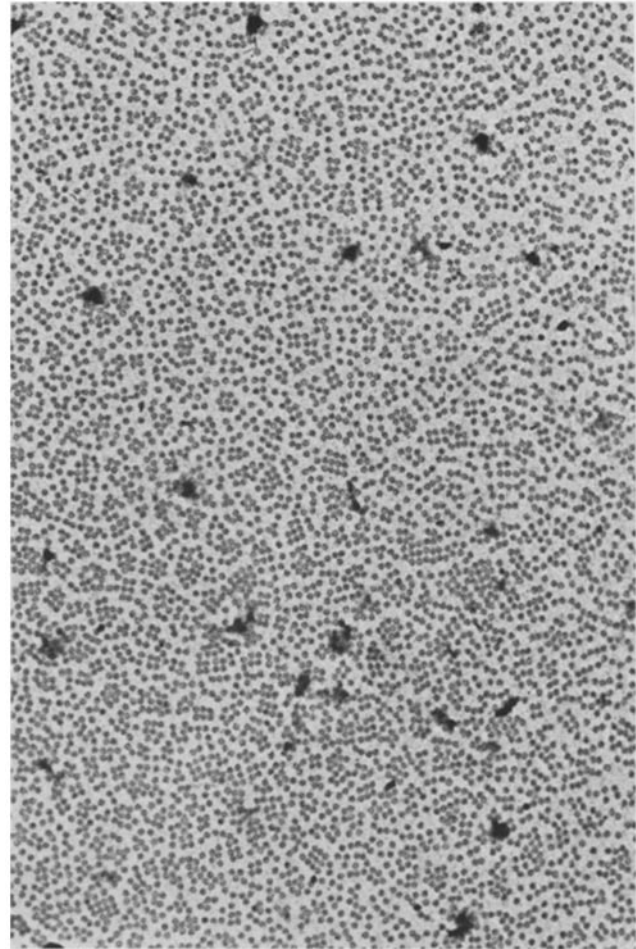


FIGURE 2 Isolated nuclear envelope from *X. laevis* spread over a carbon support film. The pore complexes are usually irregularly organized but sometimes form linear and square arrays. Unstained. $\times 8,000$.

The images were densitometered with a modified Nikon comparator (3) or Perkin-Elmer 1010A automatic microdensitometer (Perkin-Elmer Corp., Instrument Div., Norwalk, CT) to convert the optical densities into numerical arrays. The step size was $30 \mu\text{m}$, corresponding to 18 \AA at the specimen, and the array size was 256×256 points, or, in the case of the three-dimensional study, 512×512 points. Circular regions in these arrays, enclosing just the pore complex, were boxed off and Fourier transformed, using a program of the type described by DeRosier and Moore (8). The transforms, rather than the images, were used for subsequent manipulations.

Power spectra and rotationally averaged projections were calculated following Crowther and Amos (5). The power spectra are derived by calculating the weight of a specified n -fold rotational harmonic for the best image center consistent with n -fold rotational symmetry, and repeating this calculation over a range of values of n . Displayed are the relative strengths of the rotational harmonics contributing to the image, allowing an objective assessment of the degree of preservation to be made. The projection maps were derived by Fourier-Bessel synthesis of just those harmonics consistent with the observed eightfold rotational symmetry.

A three-dimensional map was calculated from an image of a pore complex attached to the nuclear membranes (Fig. 7) to determine the distribution of matter in the direction perpendicular to the membrane plane. Complex superposition of detail precluded the possibility of obtaining this information directly

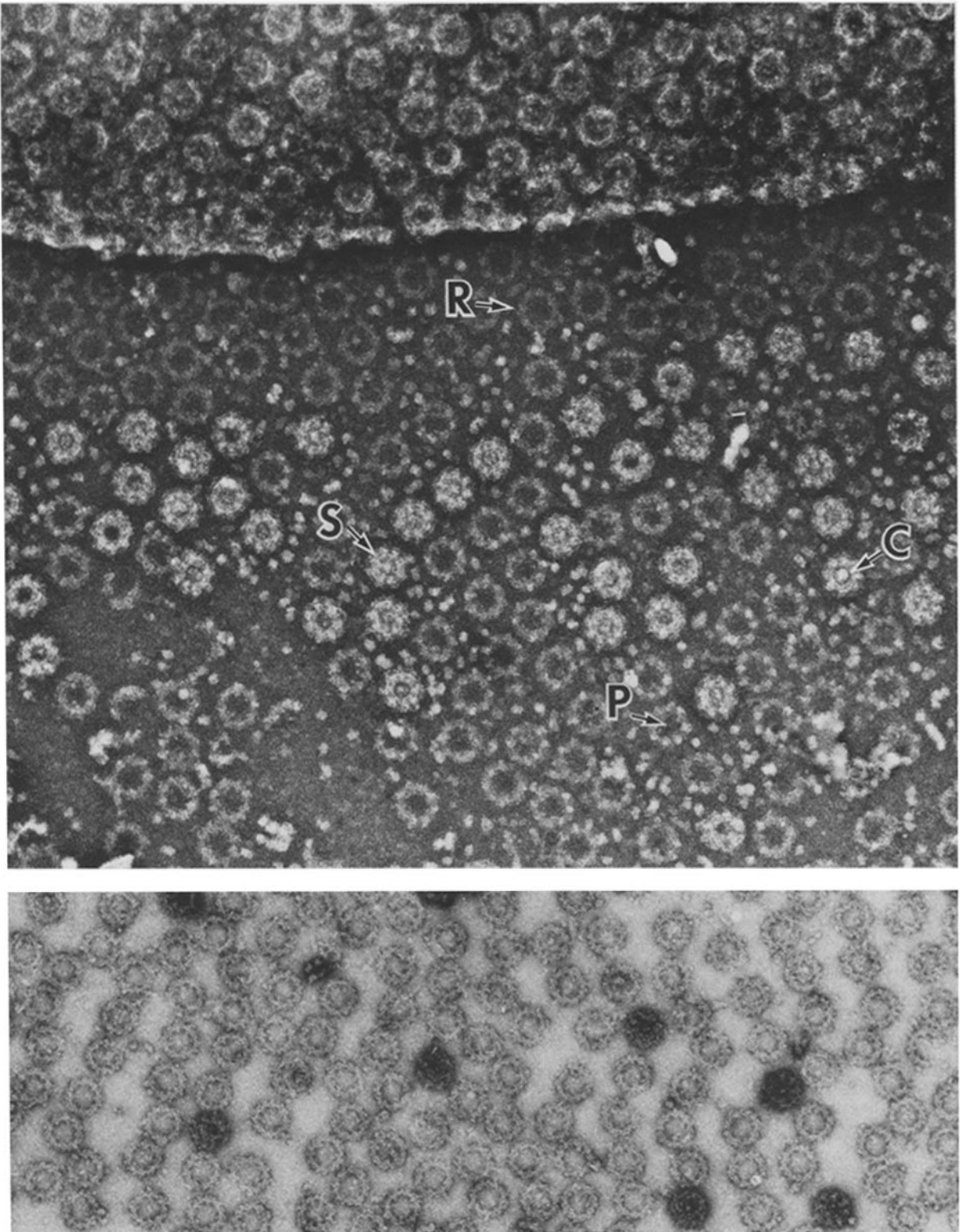


FIGURE 3 Constituents of the nuclear envelope released after its partial detachment from a polylysine-treated carbon film in the presence of 0.1% Triton X-100 (see Methods and Materials). Those constituents most obviously related to the pore complex are: rings (*R*), central plug (*C*), spokes (*S*), and particles (*P*), occasionally observed around the rings. As the lower micrograph shows, the rings are sometimes obtained in large numbers by themselves. Uranyl acetate stain. $\times 60,000$.

from different views. We manipulated the Fourier transforms as if they were derived from a two-dimensional crystal by creating an artificial reciprocal lattice consisting of lines arranged on a square grid and oriented parallel to the octad axis. Images from a tilt series were used to provide many estimates of amplitude and phase at different points along these lines, allowing the continuous variations

to be mapped out along them. The continuous curves, sampled at regular intervals, provided the Fourier terms from which to calculate the structure.

We combined the transform measurements starting with the projection data, Fig. 1, and refined the phases, image by image, in order of increasing tilt. Each image, on account of the octagonal symmetry, provided up to four independent

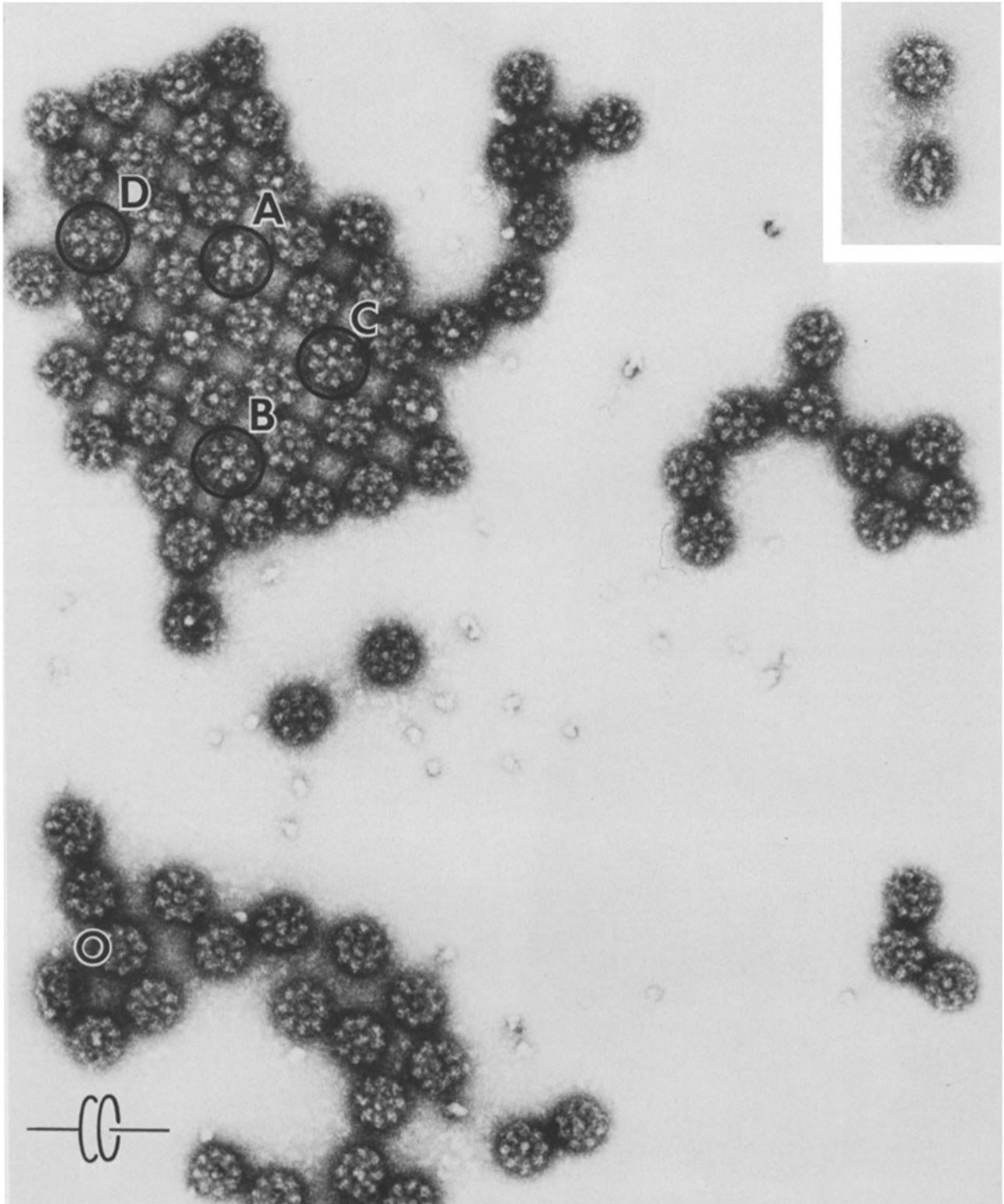


FIGURE 4 Detached pore complexes released onto the microscope grid from a nuclear envelope immersed in low salt medium containing 0.1% Triton X-100. Pore complexes within square arrays are better preserved than others. *A*, *B*, *C*, and *D* refer to images from which the results in Fig. 6 were obtained; the contributions from the eightfold harmonics are respectively 51%, 47%, 46%, and 43% of the total power associated with azimuthally varying components. Also shown are oblique, "O", and edge-on views (*inset*) of the pore complex. The drawing indicates how the view, "O", can be interpreted in three-dimensions in terms of two coaxial rings with matter lying in between them. These rings are not obvious in the *en face* views since they are thin in comparison with the rest of the structure and hence do not contribute much contrast when viewed from this direction. Uranyl acetate stain. $\times 75,000$.

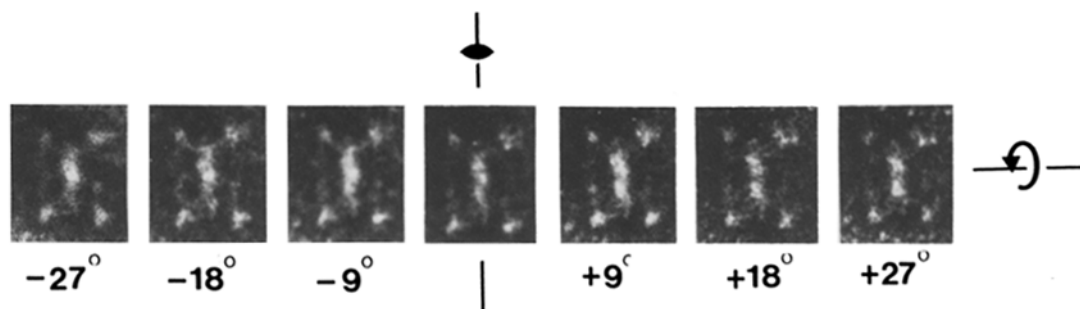


FIGURE 5 Detached nuclear pore complex tilted about the octad axis. The tilt angles are indicated. The position of the putative twofold axis is drawn for the untilted view. Uranyl acetate stain. $\times 120,000$.

estimates of amplitude and phase along each lattice line. The positions of the lattice (and eightfold related) points in the transforms were calculated from the known magnitude of tilt and the direction of the tilt axis on the micrograph. Only those phases for which the corresponding amplitudes were fairly strong ($\sim 25\%$ of the total number) and which along any given lattice line lay within $2.17 \times 10^{-4} \text{ \AA}^{-1}$ of each other were used in the refinement comparisons. The required Fourier terms were collected from the smooth amplitude and phase curves derived from these data by sampling at intervals of $4.34 \times 10^{-4} \text{ \AA}^{-1}$ along the lattice lines. Errors involved in drawing out these smooth curves caused only small departures from perfect octagonal symmetry. Further details are given in Table I.

RESULTS

Pore complexes in the nuclear envelopes of *Xenopus* oocytes occupy a large fraction of the total membrane surface. Their organization within the membranes is usually rather irregular, but they sometimes form lines or, more rarely, square arrays (Fig. 2). Such motifs are probably a result of their interaction with the thin nuclear lamina (1, 19) and with each other. A complete description of the pore complex, within the envelope, is derived below by bringing together information obtained from several types of experiment.

Plugs, Spokes, Particles, and Rings

We find that the pore complex is constructed from, or related to, several discrete constituents. These are most easily recognized following release with the detergent, Triton X-100 (see Methods and Materials), when both the separated constituents and intact pore complexes appear next to the envelope skeleton (Fig. 3). Clearly visible are: (a) "rings" which have an inside diameter close to 800 \AA and an outer diameter the same as that of the pore complex itself ($\sim 1,200 \text{ \AA}$); (b) large particles forming "plugs" at the centers of the pore complexes; (c) smaller ($\sim 220 \text{ \AA}$) particles occasionally arranged around the circumference of the rings; and (d) "spokes," matter in intact pores extending radially outwards from the plugs towards the periphery. The plugs have a diameter of up to 350 \AA , depending possibly on their state of preservation. The rings are composed of globular subunits and their power spectra display weak eightfold components (results not shown).

Detached Pore Complexes

To learn about the three-dimensional arrangement of some of these constituents we investigated further the structure of detached pore complexes. Viewed *en face* (i.e., from a direction perpendicular to the plane in which the membranes would lie) the detached pore complex is divisible into eight parts which are approximately equivalent and symmetrical about lines drawn radially (Fig. 4; see also Fig. 6). It therefore seems to display elements of both octagonal and mirror symmetry. The appearance of true mirror symmetry would suggest that it is

composed of two equal but oppositely facing halves (i.e., halves related by twofold axes perpendicular to the octad axis and lying in the central plane). Other views are in accord with this configuration. For example the oblique view, "O", in Fig. 4, shows two circular outer rims which are coaxial and equal in diameter and thickness. Views perpendicular to the octad axis (Fig. 5, and *inset* to Fig. 4) show a central zone of matter flanked by two lines (the rims seen edge-on) which are equally prominent at their extremities and symmetrically disposed on either side.

When this structure is tilted about the octad axis (Fig. 5) the rims produce only small variations in contrast and apparent diameter, except at high tilts where flattening effects (11) become most significant. This indicates that the rims are rings of approximately constant thickness rather than, say, circular arrays of the $\sim 220 \text{ \AA}$ -diameter particles. Moreover the diameter of the rims corresponds with that of the rings in Fig. 3. We thus suppose the pore complex to be framed by two equal rings facing toward the nucleus and the cytoplasm of the cell, respectively. The separation between the rings varies ($300\text{--}600 \text{ \AA}$) probably because of rather flexible, or easily distorted, connections (most obvious in the -18° and -9° tilts) to the rest of the assembly.

In the parts of the pore complex excluding the rings the changes in contrast with angle of tilt are more pronounced. At -27° (Fig. 5), for example, the central zone displays a peak of density over the octad axis, whereas at 0° the density is more evenly distributed. The distribution of matter at the extremities of this zone, where it links up with the rings, changes to a similar degree. These variations are consistent with features varying octagonally around the axis of the pore complex, although poor preservation prevents an exact correspondence of views differing in tilt by 45° .

Power spectra calculated from images of *en face* views which display strong octagonal symmetry indicate that preservation is best in "crystalline" regions, where the pore complexes lie closely apposed. Pore complexes by themselves are apparently more subject to staining distortions, involving differential shrinkage, as described by Moody (22). Best preserved pore complexes show evidence of 16- and 24-fold harmonics in addition to the basic eightfold harmonic (Fig. 6). In general, the stronger the higher order contributions relative to the background the more perfect the mirror symmetry—a phenomenon one would expect if indeed the pore complexes are constructed from two equal and oppositely facing halves.

Consistent features of the projection maps (Fig. 6) are a round central plug, eight prominent spokes emanating from it radially, and a partitioning of each spoke into characteristic regions or domains. We distinguish an inner domain at radii between 220 and 400 \AA where the spoke is narrowest and tending to connect up circumferentially with its equivalent

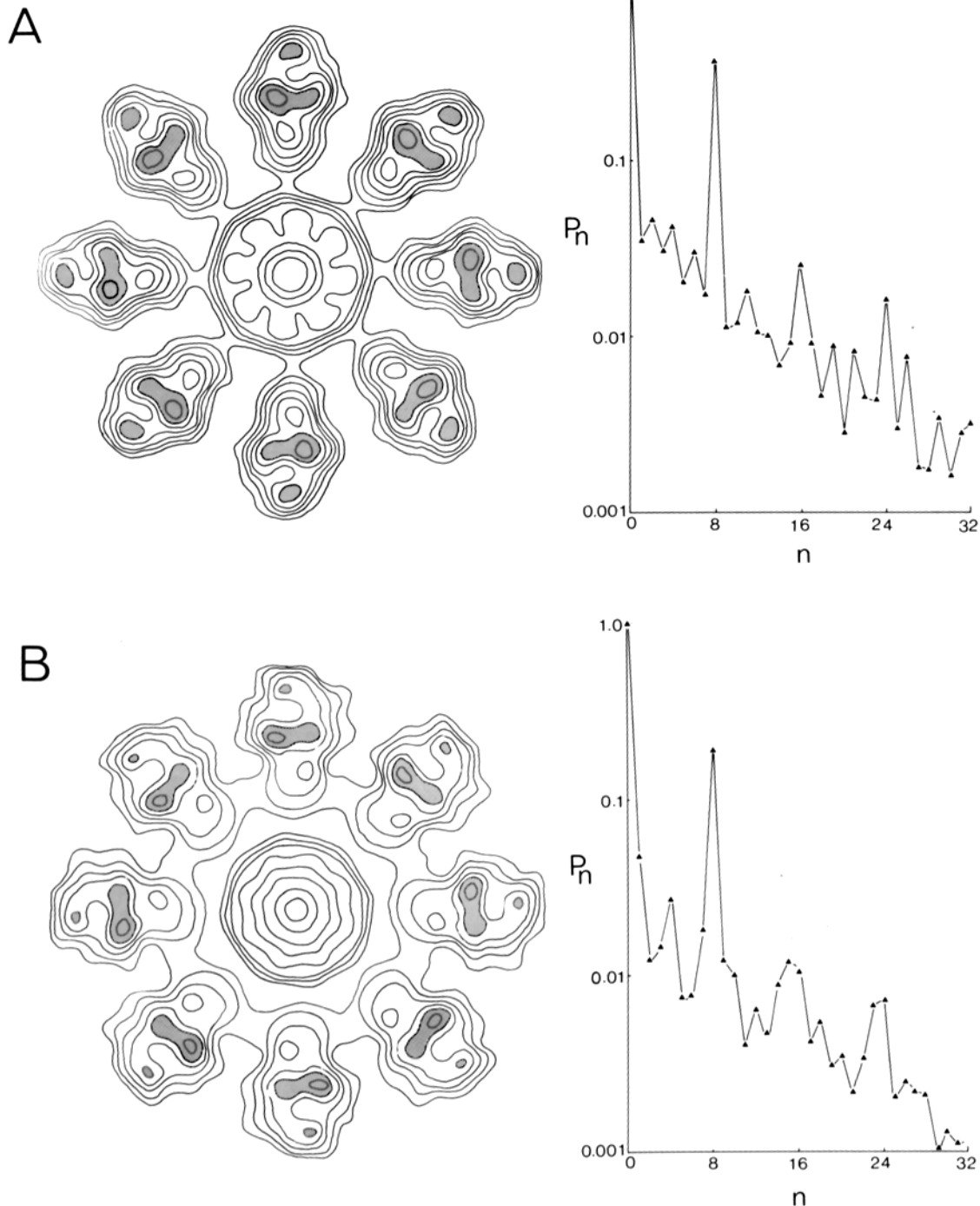


FIGURE 6 Projection maps obtained from the detached pore complexes, *A*, *B*, *C*, and *D* in Fig. 4, and their rotational power spectra, plotted on a logarithmic scale. Improvements of the power spectra in terms of enhanced 16-fold ($n = 16$) and 24-fold ($n = 24$) harmonics relative to the background level are correlated with a stronger tendency towards mirror symmetry. The consistently observed broad and sharp peaks of density (shaded) are at radii of 450 and 550 Å, respectively. The resolution is ~ 90 Å. The broken lines drawn in *D* indicate the positions of the membrane border and the particulate matter shown in Fig. 9; the two radial lines correspond to the putative twofold axes which give rise to the appearance of mirror symmetry in projection.

neighbors, and an outer domain composed of two peaks, one rather broad and the other rather sharp at radii of 450 and 550 Å, respectively. Correlation with the edge-on view suggests that the inner domain and plug are located in the central plane of the pore whereas the outer domain encompasses the region where the two oppositely facing halves of the spokes diverge from this plane to link up with the rings. The broad peak (outer domain) appears to be the part of the structure where the rings and the matter in the central plane superimpose. The

rings themselves contribute little contrast because, viewed in this direction, they are very thin in comparison to the rest of the structure. The ~ 220 Å-diameter particles observed in Fig. 3 are not a part of the isolated pore complex.

Pore Complexes Attached to Nuclear Membranes

The pore complex attached to the nuclear membranes (Fig.

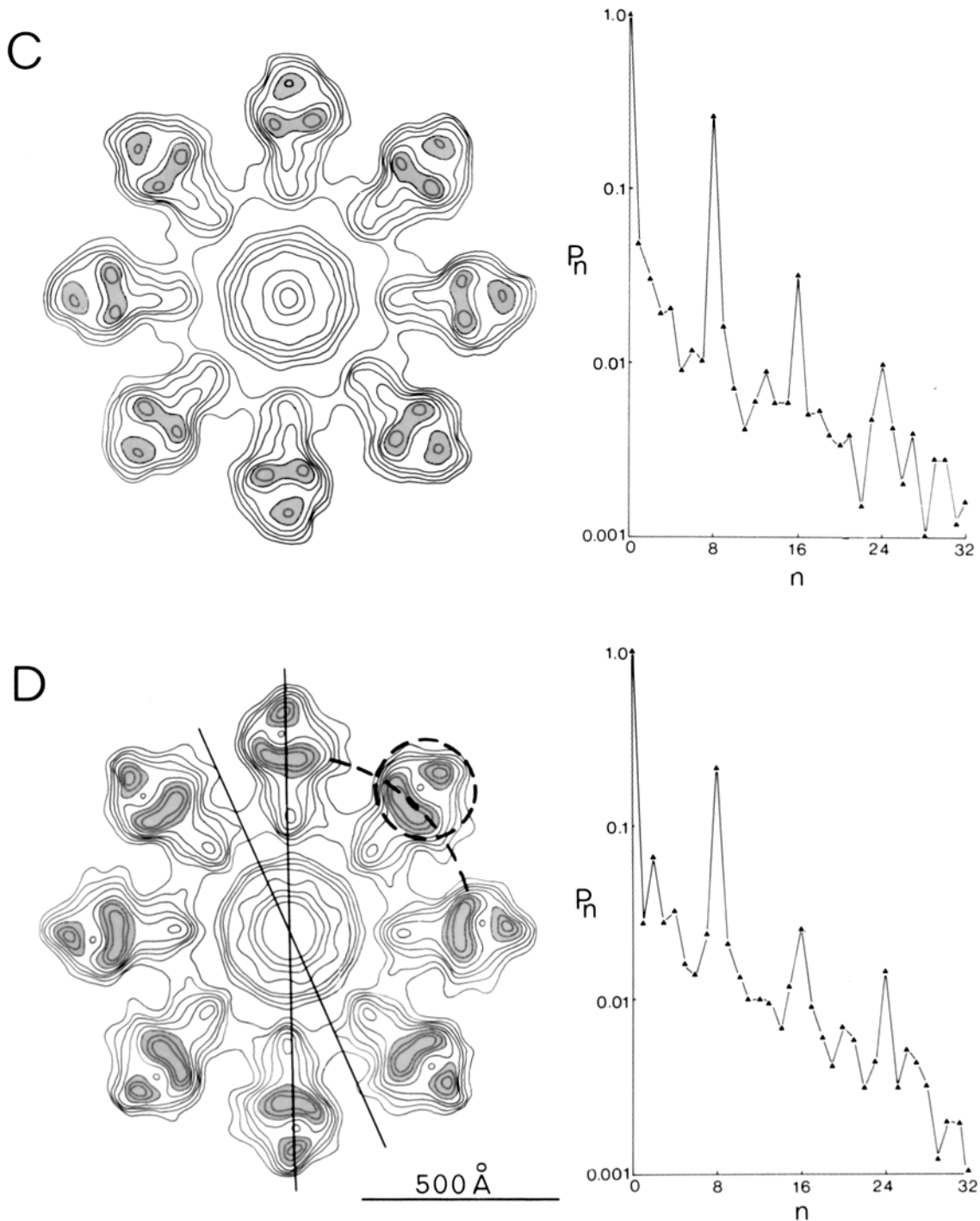


FIGURE 6 C and D

7) has additional contrast due to the two membrane layers which are contiguous and come together at the pore periphery (33). We find that the borders of these membranes are made conspicuous by incubating the nuclear envelope either in high salt medium (400 mM KCl) or in low salt medium in which the $MgCl_2$ is replaced by 1 mM EDTA (Fig. 8). The former treatment, although introducing some disorder, largely preserves the integrity of the pore complex. The latter treatment leads to its dissociation, causing also changes in the size of the membrane openings.

Comparison of Figs. 7 and 8 shows that the increased clarity of the membrane borders produced by high salt or EDTA is associated with the detachment of particles from around the

perimeters of the pore complex and from intervening spaces.

The effect of the presence of these particles and of the membrane on the appearance of the projection maps is significant only at high radius. In projection maps calculated from pore complexes attached to the nuclear membranes, Fig. 9, the spokes have more matter associated with them in their outer domain than previously (Fig. 6) and appear against a stronger background density (the membrane) beginning abruptly at a radius of ~ 450 Å.

Particles around Cytoplasmic Perimeter

A low resolution three-dimensional map of a pore complex attached to the nuclear membranes was calculated from a series

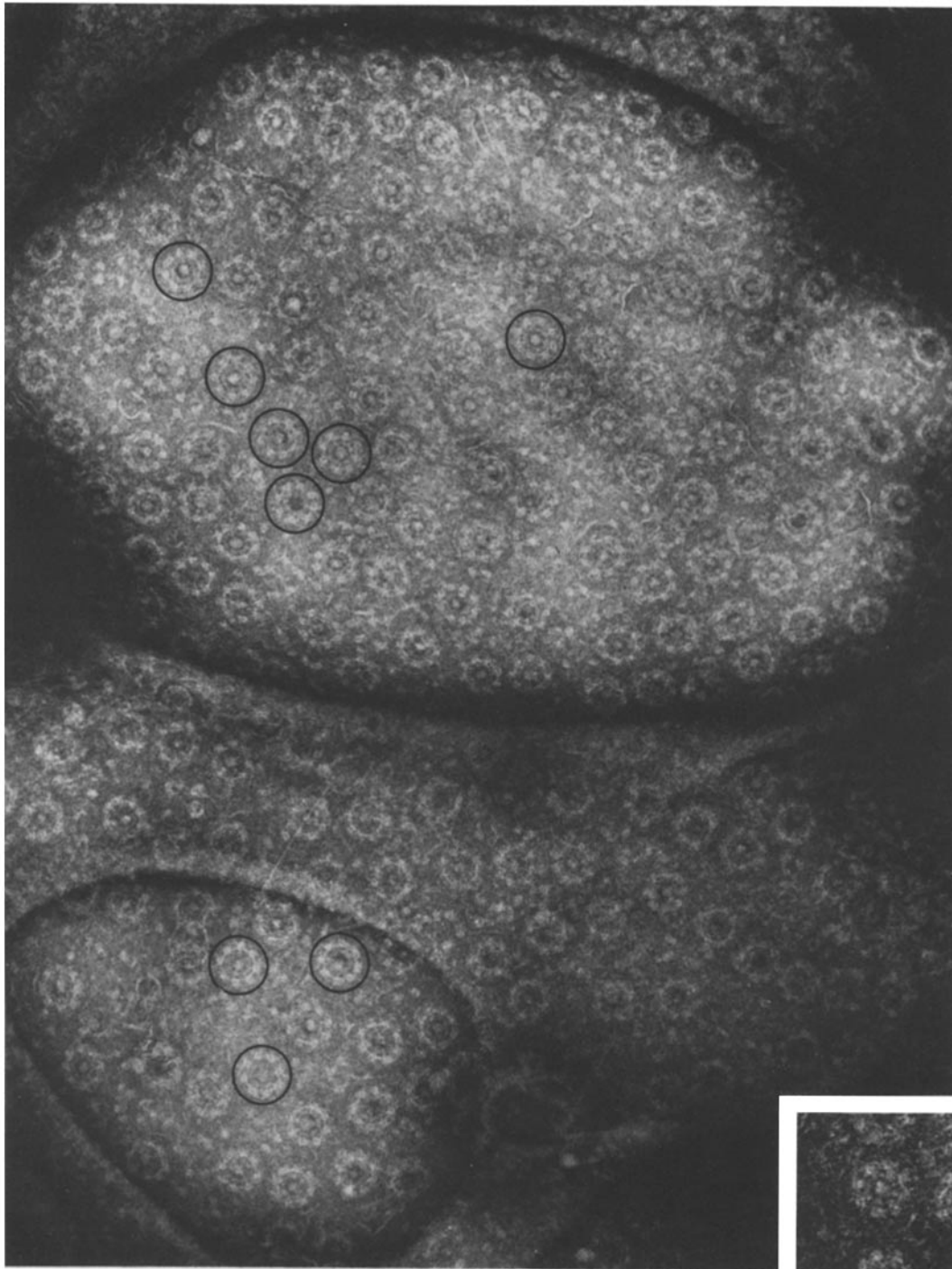


FIGURE 7 Isolated nuclear envelope spanning holes in a carbon support film. For the pore complexes encircled, the contributions from the eightfold harmonics are (top of page to bottom): 23%, 21%, 24%, 27%, 25%, 20%, 15%, 25%, 32%, and 32% of the total power associated with azimuthally varying components. The absence of a central plug in some of the pore complexes may be a consequence of the isolation procedure. The *inset* is of the image from which the results in Fig. 10 were obtained. Gold thio-glucose stain. $\times 58,000$. *Inset*, $\times 73,000$.

of images taken with different tilts (see Materials and Methods) to observe how the particulate matter superimposing with the spokes is distributed in the direction of the octad axis.

Some details of this map are given in Fig. 10. Central sections perpendicular to the plane of the membranes (Fig. 10*a*) show a marked departure from the putative twofold relationship described earlier (Fig. 5). The zone contributed by the plug and the inner domain of the spokes is now flanked, at high radius, by matter more heavily weighted towards the cytoplas-

mic half. This additional matter gives rise to strong eightfold modulations in sections parallel to the membrane plane and a strong asymmetry in terms of the variation in eightfold contrast at this radius with distance through the structure (Fig. 10*b*). Since both sides of the pore complex were exposed equally to the stain (see Materials and Methods) it is most unlikely that the asymmetry is due to this treatment.

We interpret the details to indicate that the pore complex has, on its cytoplasmic perimeter, particles—presumably the

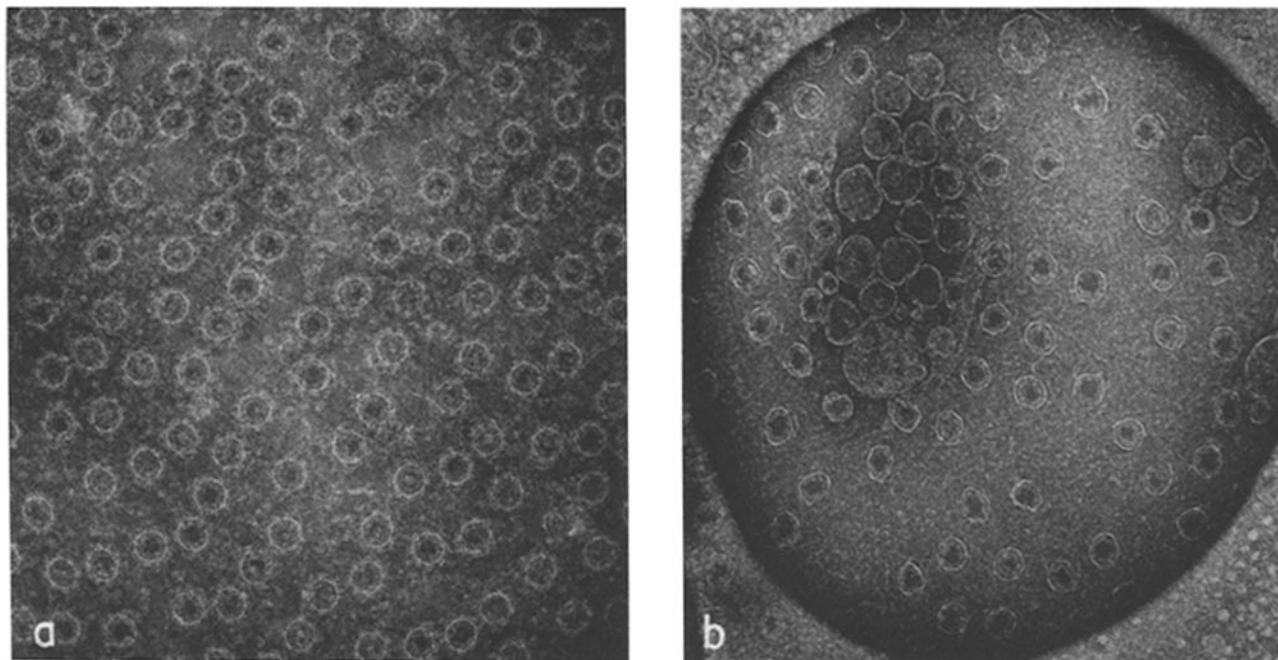


FIGURE 8 Isolated nuclear envelopes after incubation in (a) in high salt medium (400 mM KCl) and (b) 1 mM EDTA for 1 min (see Materials and Methods). Loss of matter associated with these treatments exposes the membrane borders of the nuclear pores. The diameter of the opening delineated by these borders becomes variable after treatment with EDTA. Gold thio-glucose stain over holes in the carbon support film. $\times 45,000$.

same as those in Fig. 3—which overlay the membrane, the ring and the spokes. It is unlikely that other maps would show other additional features (e.g., particles also on the nuclear side) since, of the 58 pore complexes attached to membranes which we analyzed in projection, the one from which the map was constructed exhibits the best power spectrum in terms of resolution and the strongest eightfold harmonic. On the other hand, inspection of the micrographs suggests that pore complexes often have less than eight particles on their perimeter, and sometimes none.

We confirmed the presence of these particles on the cytoplasmic side, independent of the structure analysis, by releasing them with high salt from envelopes pressed cytoplasmic face downwards onto polylysine-coated carbon films (see Materials and Methods). The “finger-prints” thus obtained show up to eight particles arranged in ~ 1000 Å diameter circles (Fig. 11). Now isolated from the envelope and the rings, the particles are easily distinguished from the round central plug, on the basis of their smaller size and more angular shape, but seem to be identical to the particles in the spaces between the rings. They also correlate closely with inactive ribosomes given the same treatments (Fig. 12), in terms of their shape and size.

DISCUSSION

The nuclear pore complex is an assembly of several discrete constituents. We have investigated their three-dimensional organization by visualizing them, at a resolution of ~ 90 Å, both in the presence of and isolated from the nuclear membranes. We used Fourier analysis methods to evaluate and average the images and to derive three-dimensional information from different views. The schematic diagram, Fig. 13, summarizes our results.

We find the pore complex to be a symmetrical structure framed by two widely separated, coaxial rings. The rings attach to the two nuclear membranes so that one faces the nucleus

and the other the cytoplasm of the cell. Connected to these rings and extending radially inwards from them, along a central plane, are elongated structures which we call spokes. They approach and appear to contact a central large, approximately spherical particle, the plug. Cytoplasmic particles, also observed decorating the perimeter of many of the pore complexes, are probably not integral components since they are easily detached and are only there when the nuclear membranes are present.

The structural framework of the assembly, i.e., the rings, the spokes, and their connecting links, appears to be arranged with octagonal symmetry about the central axis perpendicular to the plane of the membranes and with twofold symmetry about axes lying in this plane (giving the dihedral point group D_8 [822]). A configuration like this, in which the two halves of the assembly face in opposite directions, would account simply for observations of single pore complexes spanning the two equivalent, but oppositely facing, membranes of ER cisternae (13). An example of another two-layered membrane system incorporating this design principle would be the gap junction (29).

Some earlier models for the pore complex show eight equal “granular subunits” around its perimeter on both the nuclear and cytoplasmic sides (12, 26) and so may be construed as suggesting a twofold symmetry relationship. However, the quality of preservation achieved in the earlier studies was not assessed and alternative interpretations could not therefore be discounted. We suggest that the granular subunits and likewise the proposed tubular subunits (30) or microcylinders (35) should be identified with the detail which we observe in the region where the spokes connect to the rings. It is easy to see how this detail could be interpreted in various ways according to the state of preservation. The features we find in the peripheral region of the pore complex (Figs. 4 and 5) are particularly distinct because we have exposed them by taking away the membranes.

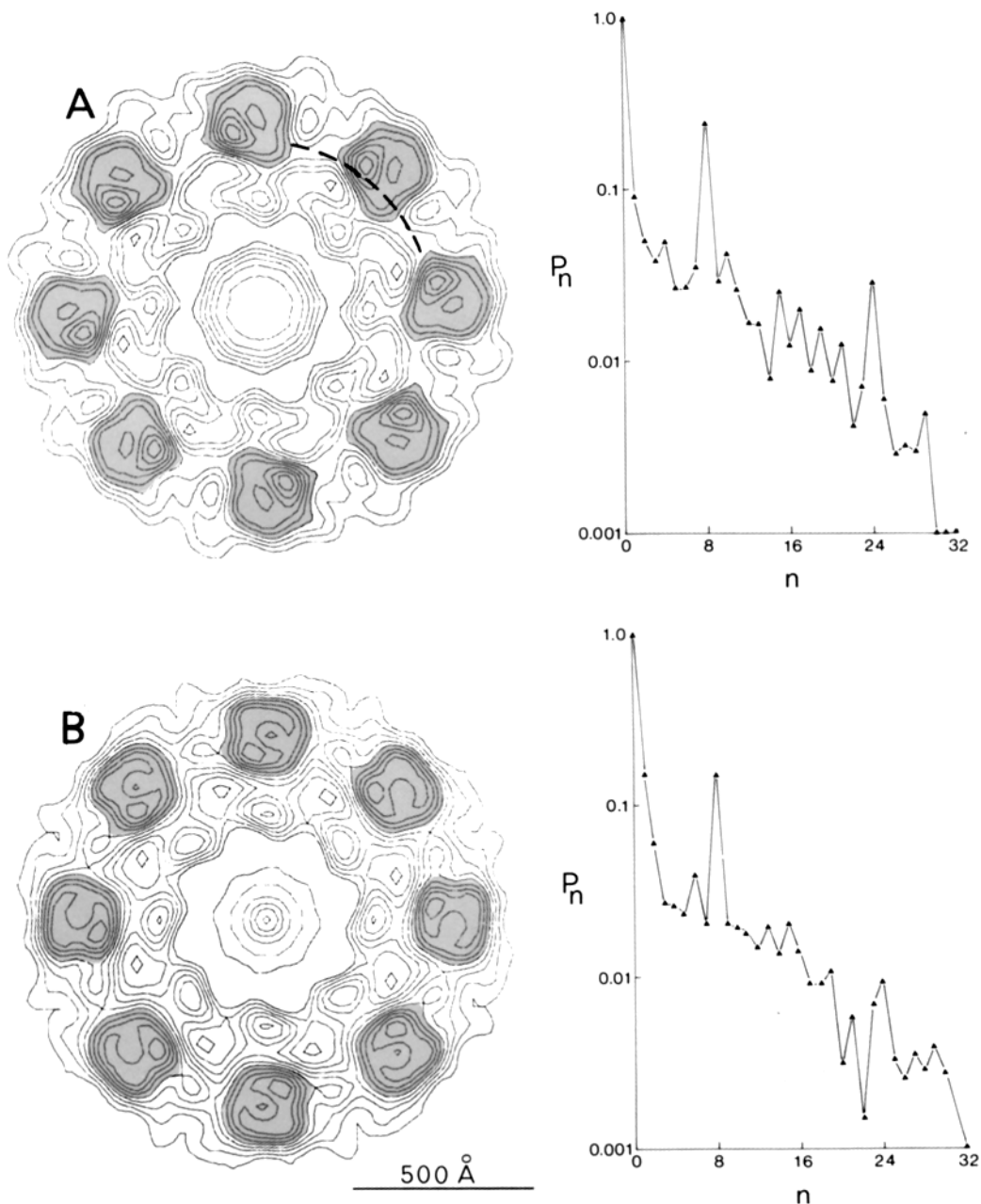


FIGURE 9 Typical projection maps from pore complexes attached to the nuclear membranes, and their rotational power spectra. The resolution is about 90 Å. The shading indicates the position of the particulate matter not present in images of the isolated pore complexes. The broken line in (A) indicates the position of the membrane border. The view is from the cytoplasm towards the nucleus. Power spectra of pore complexes attached to the nuclear membranes show 8- and 24-fold harmonics but the 16-fold harmonic is always very weak or absent.

Several independent lines of evidence have led to our conclusion, Fig. 13, that in the cell there are sometimes large (~220 Å-diameter) particles decorating the pore complex around its perimeter on the cytoplasmic side. First, such particles were present on occasions around the rings, following their detachment from the nuclear envelope with Triton X-100 (Fig. 3). Second, these particles were too large to be accommodated as part of the structure of the pore complex itself, yet did give rise to additional density over the rings and spokes of pore complexes which had not been detached from the nuclear envelope. Third, we demonstrated by a three-dimensional analysis that the additional density was concentrated toward the cytoplasmic side rather than the central plane or the side of the nucleus.

Fourth, we were able to detach these particles (identified by their appropriate circular configuration) by contact of the cytoplasmic surface of the nuclear envelope against the microscope grid.

At least two reports (6, 17) have clearly demonstrated decoration of the pore perimeter by particles which might be the same as those we observe. In other careful studies (e.g., reference 31), such particles have not been detected, despite conditions being used which should have allowed their retention. Thus the particles appear to be there *in vivo* on some occasions but not on others. Accordingly, their presence may be related to a process such as the activity of the pore in mediating transfer of molecules between nucleus and cytoplasm.

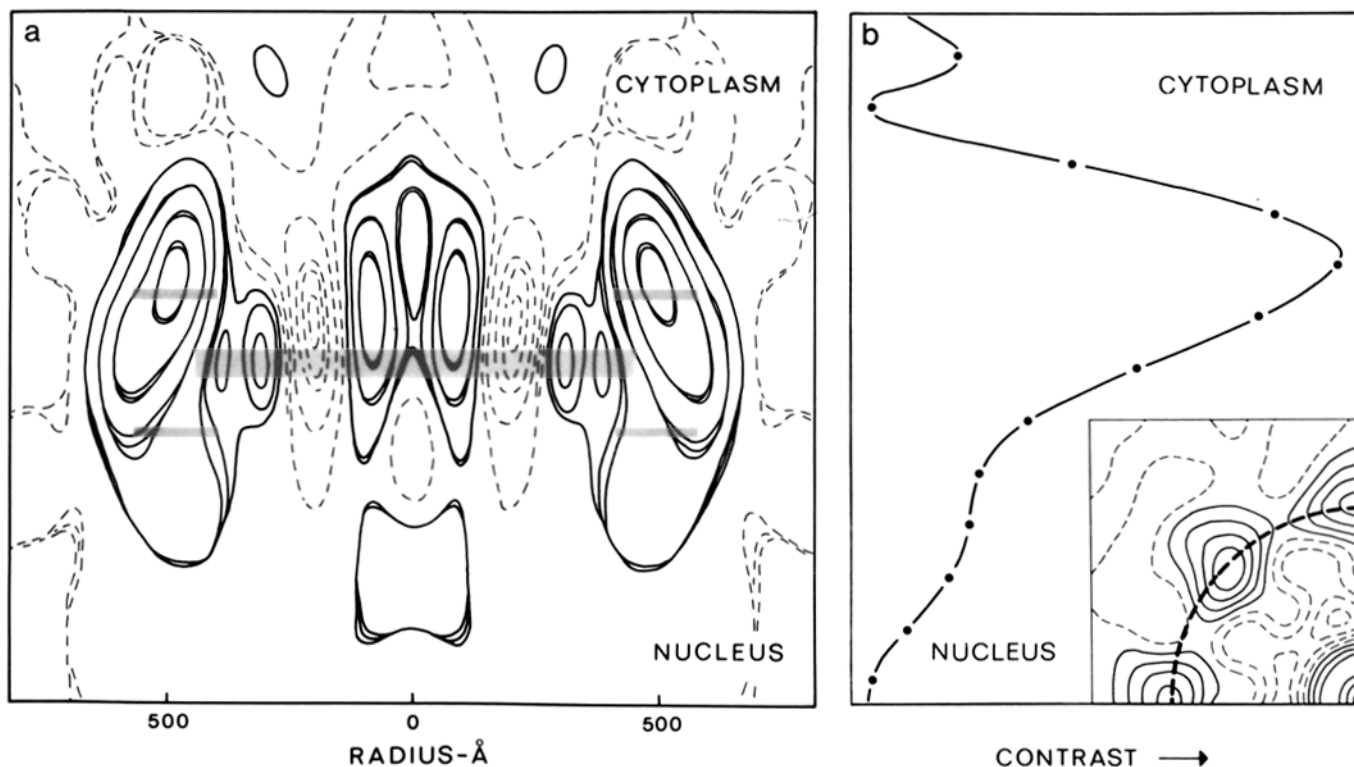
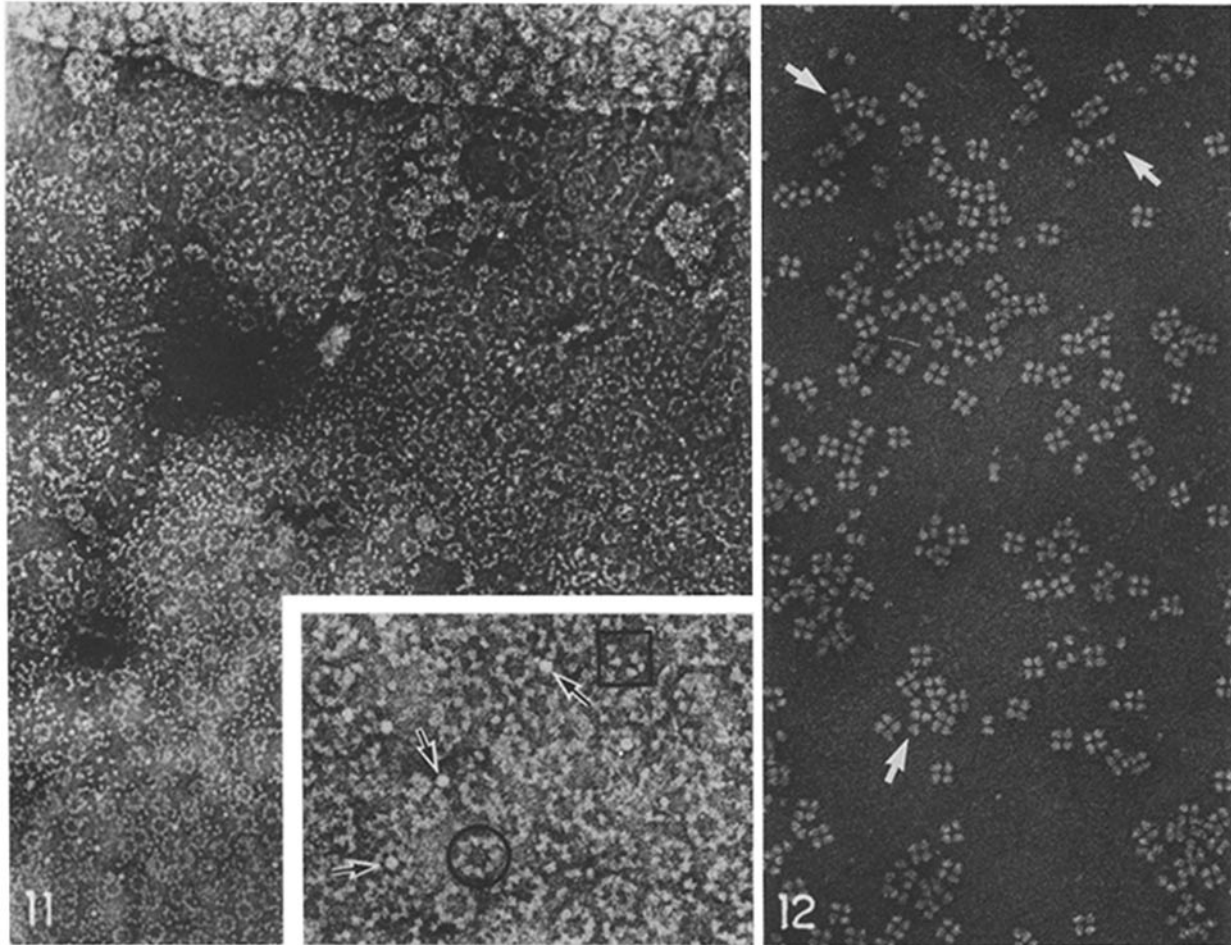


FIGURE 10 Details of a low resolution three-dimensional analysis of a pore complex attached to the nuclear membranes. (a) A projection of 25-Å thickness through the three-dimensional map built up from sections perpendicular to the plane of the membranes and intersecting the maxima in the eightfold density modulations. The full lines are the positive contours indicating the regions where the biological matter is concentrated. The broken lines are negative contours. The shading indicates the estimated positions of the twofold related features described earlier (Fig. 5). The two membrane layers are not resolved. Features on the cytoplasmic side give rise to strong eightfold modulations, but those on the nuclear side do not. (b) A plot of the variation in contrast associated with the eightfold modulations at a radius of 500 Å. The vertical scale is the same as in a. The contrast was estimated as the difference between the maximum and minimum densities in sections perpendicular to the octad axis. The line at the 500-Å radius along which the densities were measured is indicated in the section giving maximum contrast, at the bottom of the figure. There is marked asymmetry in contrast compared to similar views from detached pore complexes. This analysis gives only a qualitative idea of the relative levels and strengths of features. The Fourier terms giving the variation in mean density along the direction of the octad axis are not included. Dimensions of features in this direction are also affected by flattening distortions (19). Because of the variable preservation of the central plug, we attach no significance to details in this region.



FIGURES 11 and 12 "Finger-print" of material detached from the cytoplasmic surface of the nuclear envelope (top of picture) onto a polylysine-coated carbon support film. The detachment was achieved using high potassium concentration (400 mM; see Methods and Materials). The somewhat angular particles arranged in rings (circle) or randomly (square) can be identified with those in Fig. 7 around the perimeter of the pore complexes and in intervening spaces. These particles are easily distinguished from the larger, round, central plug (arrows). Gold thio-glucose stain. $\times 25,000$. *Inset*, $\times 55,000$. Fig. 12: Ribosomes isolated from hypothermic chick embryos, after incubation in high salt, fixation, and staining as in Fig. 11. Both the tetrameric and single ribosomes appear rather angular (arrows), possibly as a result of detachment of the small subunit. $\times 55,000$.

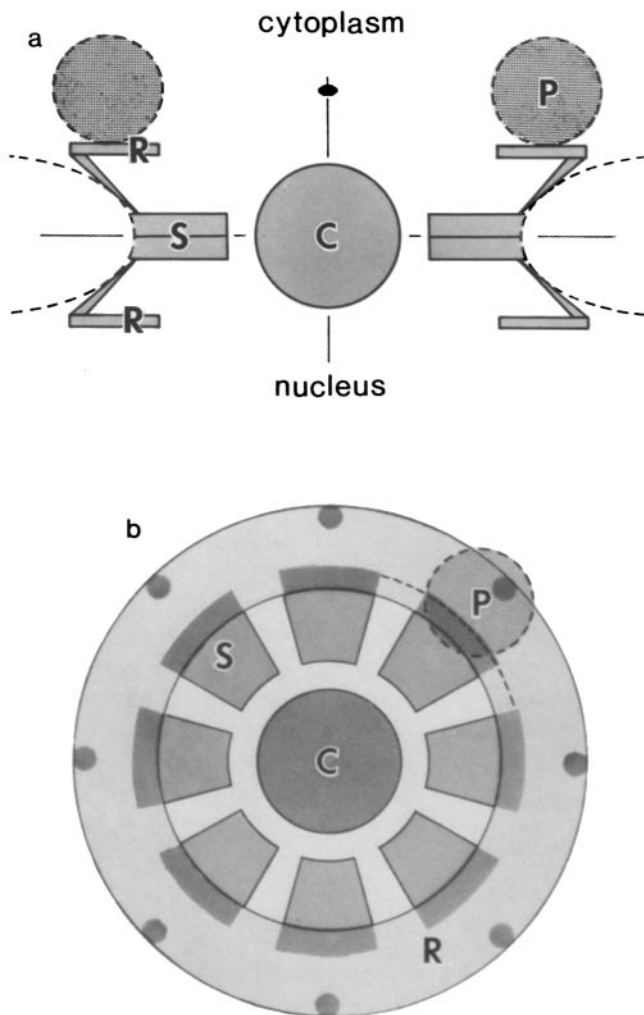


FIGURE 13 Diagram of the nuclear pore complex: (a) In central cross-section and (b) in projection down the octad axis. The major constituents are the central plug (C), the spokes (S), and the rings (R). The spokes are connected to the rings near to the maximum radius of the assembly (~600 Å). Superposition of detail in projection gives rise to a characteristic hollow or bilobed region of density near the outer extremity of the spokes (see Fig. 6). The broken lines outline the positions of the additional features present with pore complexes embedded within the nuclear envelope: the two membrane layers which come together at the pore complex and octagonally arranged particles (P), resembling ribosomes. The position of the membrane border in a corresponds with the thin-section view (e.g., reference 6). The particles are easily detached and are not always present.

Our observations on the character of these particles are consistent with the surmise that ribosomes (21, 31), or alternatively ribosomal precursors, are sometimes associated with the nuclear pore complex. The particles resemble inactive ribosomes stained under identical conditions (Figs. 11 and 12). They also resemble the membrane-bound particles in the spaces between the pores, which from studies of nuclear envelopes in other cells one would presume to be ribosomes (25, 31, 32). That they are detached from the periphery of the pore complex by the same biochemical treatments (addition of Triton X-100, EDTA, or a high concentration of potassium ions) that release inactive ribosomes from membranes in secretory cells (2, 27) could reflect the fact that they are attached directly to the

nuclear membrane in the immediate vicinity of the pore complex and interact only weakly with the pore complex itself.

We are grateful to John Gurdon and Rick Bram for generously providing us with oocytes, and to Tony Crowther and Linda Amos for the use of their rotational averaging computer program. We thank Roger Kornberg, John Murray, and John Kilmartin for valuable discussions and comments. Guido Zampighi suggested using gold thio-glucose as a negative stain.

Received for publication 14 July 1981, and in revised form 21 October 1981.

REFERENCES

- Aaronson, R. P., and G. Blobel. 1975. Isolation of nuclear pore complexes in association with a lamina. *Proc. Natl. Acad. Sci. U. S. A.* 72:1007-1011.
- Adelman, M. R., D. D. Sabatini, and G. Blobel. 1973. Ribosome membrane interaction. Nondestructive disassembly of rat liver rough microsomes into ribosomal and membranous components. *J. Cell Biol.* 56:202-229.
- Arndt, U. W., J. Barrington-Leigh, J. F. W. Mallet, and K. E. Twinn. 1969. A mechanical microdensitometer. *J. Sci. Instrum.* 2:385-387.
- Bonner, W. M. 1975. Protein migration into nuclei I. Frog oocyte nuclei in vivo accumulate microinjected histones, allow entry to small proteins, and exclude large proteins. *J. Cell Biol.* 64:421-430.
- Crowther, R. A., and L. A. Amos. 1971. Harmonic analysis of electron microscope images with rotational symmetry. *J. Mol. Biol.* 60:123-130.
- Daniels, E. W., J. M. McNiff, and D. R. Ekberg. 1969. Nucleopores of the giant amoeba, *Pelomyxa carolinensis*. *Z. Zellforsch. Mikrosk. Anat.* 98:357-368.
- DeRobertis, E. M., R. F. Longthorne, and J. B. Gurdon. 1978. The intracellular migration of nuclear proteins in *Xenopus* oocytes. *Nature (Lond.)* 272:254-256.
- DeRosier, D. J., and P. B. Moore. 1970. Reconstruction of three-dimensional images from electron micrographs of structures with helical symmetry. *J. Mol. Biol.* 52:355-369.
- Fabergé, A. C. 1973. Direct demonstration of eightfold symmetry in nuclear pores. *Z. Zellforsch. Mikrosk. Anat.* 136:183-190.
- Feldherr, C. M., and J. M. Marshall. 1962. The use of colloidal gold for studies of intracellular exchanges in amoeba *Chaos chaos*. *J. Cell Biol.* 12:641-645.
- Finch, J. T., and A. Klug. 1965. The structure of viruses of the Papilloma-Polyoma type. III. Structure of rabbit Papilloma virus. *J. Mol. Biol.* 13:12.
- Franke, W. W., and U. Scheer. 1970. The ultrastructure of the amphibian envelope of amphibian oocytes: a reinvestigation. *J. Ultrastruct. Res.* 30:288-316.
- Franke, W. W., U. Scheer, and H. Fritsch. 1972. Intracellular and cytoplasmic annulate lamellae in plant cells. *J. Cell Biol.* 53:823-827.
- Gall, J. G. 1967. Octagonal nuclear pores. *J. Cell Biol.* 32:391-399.
- Gurdon, J. B. 1976. Injected nuclei in frog oocytes: fate, enlargement, and chromatin dispersal. *J. Embryol. Exp. Morphol.* 36:523-540.
- Gurdon, J. B. 1970. Nuclear transplantation and the control of gene activity in animal development. *Proc. R. Soc. Lond. B Biol.* 176:303-314.
- Hoefjmakers, J. H. J., J. H. N. Schel, and F. Wanka. 1974. Structure of the nuclear pore complex in mammalian cells. Two annular components. *Exp. Cell Res.* 87:195-206.
- Huxley, H. E., and G. Zubay. 1960. Electron microscope observations on the structure of microsomal particles from *Escherichia coli*. *J. Mol. Biol.* 2:10-18.
- Krohne, G., W. W. Franke, and U. Scheer. 1978. The major polypeptides of the nuclear pore complex. *Exp. Cell Res.* 116:85-102.
- Martini, D. H. W., and H. J. Gould. 1975. Molecular weight distribution of ribosomal protein from several vertebrate species. *Mol. Gen. Genet.* 142:317-331.
- Mepharm, R. H., and G. R. Lane. 1969. Nucleopores and polyribosome formation. *Nature (Lond.)* 221:288-289.
- Moody, M. F. 1971. Application of optical diffraction to helical structures in the bacteriophage tail. *Philos. Trans. R. Soc. Lond. B Biol. Sci.* 261:181-195.
- Morimoto, T., G. Blobel, and D. D. Sabatini. 1972. Ribosome crystallization in chicken embryos. I. Isolation, characterization, and in vivo activity of ribosome tetramers. *J. Cell Biol.* 52:338-354.
- Paine, P. L., L. C. Moore, and S. B. Horowitz. 1975. Nuclear envelope permeability. *Nature (Lond.)* 254:109-114.
- Palade, G. E. 1955. A small particulate component of the cytoplasm. *J. Biophys. Biochem. Cytol.* 1:59-68.
- Roberts, K., and D. H. Northcote. 1970. Structure of the nuclear pore in higher plants. *Nature (Lond.)* 228:385-386.
- Sabatini, D. D., Y. Tashiro, and G. E. Palade. 1966. On the attachment of ribosomes to microsomal membranes. *J. Mol. Biol.* 19:503-524.
- Scheer, U. 1972. The ultrastructure of the nuclear envelope of amphibian oocytes. IV. On the chemical nature of the pore complex material. *Z. Zellforsch. Mikrosk. Anat.* 127:127-148.
- Unwin, P. N. T., and G. Zampighi. 1980. Structure of the junction between communicating cells. *Nature (Lond.)* 283:545-549.
- Vivier, E. 1967. Observations ultrastructurales sur l'enveloppe nucléaire et ses pores chez des sporozoaires. *J. Microscopie.* 6:371-390.
- Watson, M. L. 1959. Further observations of the nuclear envelope of the animal cell. *J. Biophys. Biochem. Cytol.* 6:147-156.
- Watson, M. L. 1955. The nuclear envelope. Its structure and relation to cytoplasmic membranes. *J. Biophys. Biochem. Cytol.* 1:257-270.
- Watson, M. L. 1954. Pores in the mammalian nuclear membrane. *Biochim. Biophys. Acta.* 15:475-479.
- Williams, R. C. 1977. Use of polylysine for adsorption of nucleic acids and enzymes to electron microscope specimen films. *Proc. Natl. Acad. Sci. U. S. A.* 74:2311-2315.
- Wischnitzer, S. 1958. An electron microscope study of the nuclear envelope of amphibian oocytes. *J. Ultrastruct. Res.* 1:201-222.